IEEE Open Journal of
Circuits and Systems

Received 8 August 2020; revised 2 November 2020; accepted 19 November 2020. Date of current version 8 January 2021.

Digital Object Identifier 10.1109/OJCAS.2020.3041239

Performance Comparison of Baseband Signaling and Discrete Multi-Tone for Wireline Communication

JHOAN SALINAS [1] (Graduate Student Member, IEEE), JEREMY COSSON-MARTIN[1] (Student Member, IEEE), MIAD LAGHAEI[1] (Student Member, IEEE), HOSSEIN SHAKIBA[2] (Senior Member, IEEE), AND ALI SHEIKHOLESLAMI [1] (Senior Member, IEEE)

[1] Edward S. Rogers Sr. Department of Electrical and Computer Engineering, University of Toronto, Toronto, ON M5S 3G4, Canada

[2] HiLink, Huawei Technologies Canada, Markham, ON L3R 5A4, Canada

This article was recommended by Associate Editor P. H. Hsieh.

CORRESPONDING AUTHOR: J. SALINAS (e-mail: jsalinas@ece.utoronto.ca)

This work was supported in part by Huawei Technologies Canada and in part by the Natural Sciences and Engineering Research Council (NSERC) of Canada.

ABSTRACT Limits of data rate over a wireline channel depend on the channel characteristics, the signaling or modulation scheme, and the complexity one can afford for its implementation. This article compares two signaling schemes, namely baseband and discrete multi-tone (DMT), for two example channels, one with a smooth frequency response and one with a notch frequency response, to examine how far each can push the data rate towards the maximum achievable data rate, derived from Shannon Capacity formula.

INDEX TERMS Discrete multi-tone (DMT), pulse amplitude modulation (PAM), quadrature amplitude modulation (QAM), Shannon's capacity, bit loading, salz SNR, integrated crosstalk noise (ICN), insertion loss (IL).

I. INTRODUCTION

THE DEMAND for higher data rates has been on the rise over the past few decades, but has seen a dramatic increase in recent months as more people resort to the Internet both for entertainment and work during the pandemic. At the chip level, this demand translates to higher bandwidth per wireline channel connecting two adjacent microchips on the same board or on daughter boards sharing the same backplane. Today, research papers report data rates of 112Gb/s/channel [1], [2] and pursue innovations to double this data rate.

It is well known that wireline channels suffer from impairments such as frequency-dependent attenuation, reflections, crosstalk, and jitter, among others. Despite these impairments, engineers have been able to increase the data rate far beyond the 3 dB bandwidth of the channel. This progress has been made by development in channel design (materials, connectors, manufacturing), innovative circuit design of equalizers, crosstalk cancellation, and clock and data recovery, as well as the choice of modulation scheme.

Today, 100 Gb/s communication per channel is achieved using digital pre-equalizers and DAC at the transmitter [3] and a combination of CTLE, ADC, and digital equalizer at the receiver. This data rate is achieved in conjunction with PAM-4 modulation [1] and in combination with partial response signaling [4]. However, a question still remains as to how far we can push the data rate without sacrificing the bit error rate for a given channel and its impairments. In addition, it remains unclear the potential of other modulation schemes such as PAM-8 or Discrete Multi-tone (DMT), which has gained attention after the implementation reported in [5], to push the data rates higher without increasing the implementation complexity (e.g., requiring large area, more power, etc.). This article attempts to answer these questions by (a) finding the limits of signaling, given the channel constraints, using Shannon's capacity theorem, and by (b) comparing baseband signaling (such as PAM-4 and PAM-8) against DMT signaling in terms of achievable data rate and complexity.

Previous publications report methods to estimate the maximum achievable rate. For example, [6] evaluates baseband PAM-M modulation, including different noise sources and implementation constraints such as noise, jitter, and slicer resolution in the context of a mixed-signal link. In the DMT case, [7] shows an achievable data rate study, where impairments such as ADC resolution, noise, residual ISI, and clipping are considered. In this article, we perform a comparison in the context of a DAC/ADC-based link. We include for both modulations the effect of crosstalk, AWGN, TX and RX jitter, residual ISI, DAC/ADC quantization noise, and clipping.

The paper is organized as follows: Section II explains how to calculate the capacity of a channel with Additive White Gaussian Noise (AWGN) and crosstalk. Sections III and IV describe our proposed method to calculate the achievable data rate, including the primary impairments in DMT and PAM, respectively. Section V covers simulation results and comparisons between DMT and baseband PAM modulation. Finally, Section VI concludes the paper.

II. BACKGROUND: CAPACITY CALCULATION

This Section describes some basic concepts of information theory and how capacity can be calculated for a frequency selective channel with crosstalk and AWGN.

A. CAPACITY

A fundamental concept in information theory is capacity, which represents the maximum number of bits per symbol that can be sent over a channel with an arbitrarily small probability of error [8]. In particular, given a memoryless continuous channel subject to AWGN with variance σ_n^2 and average transmit power P_o, the capacity, in bits per symbol, C_s, is given by the famous formula [9]:

$$C_s = \frac{1}{2}\log_2(1+\text{SNR}), \tag{1}$$

where $\text{SNR} \triangleq P_o/\sigma_n^2$ corresponds to the signal to noise ratio.

By virtue of the Nyquist's sampling theorem, the discrete-time result from (1) can be extended to the continuous-time AWGN channel with bandwidth W and signal to noise ratio SNR. For both baseband or pass-band transmission, the capacity, in bits per second, can be written as [9]:

$$C = W\log_2(1+\text{SNR}) \tag{2}$$

The capacity from (2) is modified with an SNR margin, Γ, to estimate the maximum bit rate with uncoded modulation, maintaining certain symbol error probability [10]:

$$b = W\log_2\left(1+\frac{\text{SNR}}{\Gamma}\right) \tag{3}$$

Γ is referred to as Gap to Capacity and is a function of the coding scheme and the symbol error probability P_e. For uncoded PAM or QAM, the value of Γ can be estimated according to:

$$\Gamma = \frac{1}{3}\left[Q^{-1}\left(\frac{P_e}{N_e}\right)\right]^2 \tag{4}$$

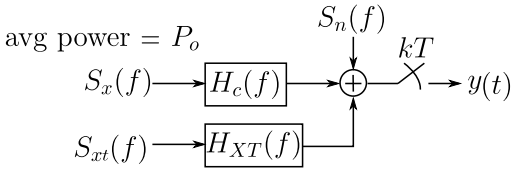

FIGURE 1. A model for a frequency-dependent channel with crosstalk and noise.

where N_e is the average number of nearest neighbor symbols, which is 2 for PAM and 4 for QAM [10], and Q^{-1} is the inverse of the Q-function, defined by $Q(x) \triangleq \frac{1}{\sqrt{2\pi}}\int_x^\infty e^{-t^2/2}dt$.

B. FREQUENCY-DEPENDENT CHANNEL

Equation (3) assumes SNR is constant across the frequency range of interest. However, in reality, channel attenuation and SNR are frequency-dependent. Typically, the high-frequency content of the transmit signal is attenuated more than its low-frequency content. To accommodate this frequency-dependent behavior in our capacity equation, we assume the model shown in Fig. 1. Here, we assume a signal with average power P_o and power spectral density (PSD) $S_x(f)$ is sent through a channel with insertion loss[1] $H_C(f)$. The received signal is affected by noise with spectral density $S_n(f)$, and (far-end/near-end) crosstalk aggressors with a PSD denoted by $S_{xt}(f)$ that is shaped by a transfer function $H_{XT}(f)$.

When the channel frequency response is non-constant, it can be divided into small sub-bands Δf, such that the channel frequency response can be considered flat for Δf. Assuming identical transmitters in the victim and aggressor lines, $S_x(f) = S_{xt}(f)$, and white noise[2] $S_n(f) = \frac{N_o}{2}$, the signal to noise ratio as a function of frequency can be written as:

$$\text{SNR}(f) = \frac{S_x(f)|H_C(f)|^2}{S_x(f)|H_{XT}(f)|^2 + \frac{N_o}{2}} \tag{5}$$

Accordingly, the total achievable rate can be written as:

$$C_{total} = sup\int_{\mathcal{B}}\log_2\left(1+\frac{\text{SNR}(f)}{\Gamma}\right)df, \tag{6}$$

where $\mathcal{B}$ represents the frequency band of interest, and *sup* represents the maximum the integral can take over all possible $S_x(f)$ that satisfy

$$2\int_0^\infty S_x(f)df = P_o \tag{7}$$

Equations (6) and (7) state that, for a given channel, there is a particular transmit power spectral density ($S_x(f)$) that maximizes the data rate through the channel. Using

1. Sanders [11] explains how the effect of reflections can be included by taking the worst-case transmitter and receiver return loss. With a conversion from S-parameters to transmission parameters, matrix multiplication, and reconversion to S-parameters, it is possible to obtain an overall transfer function $H_c(f)$ that includes the effect of reflections.

2. Under certain conditions, this term can be modified to include some impairments such as CTLE input-referred noise, ADC comparator offset or supply noise.

the Euler-Lagrange technique, Kalet and Shamai [12] found this optimum $S_x(f)$ is a solution to the following quadratic equation:

$$aS_x^2(f) + bS_x(f) + c = 0 \tag{8}$$

where:

$$\begin{aligned} a &= |H_{XT}(f)|^2\Big[|H_{XT}(f)|^2 + |H_C(f)|^2\Big] \\ b &= \frac{N_o}{2}\Big[2|H_{XT}(f)|^2 + |H_C(f)|^2\Big] \\ c &= \left(\frac{N_o}{2}\right)^2 - \frac{1}{\lambda}\frac{N_o}{2}|H_C(f)|^2 \end{aligned} \tag{9}$$

The value of the Lagrange multiplier λ is chosen to satisfy (7). Hence, to evaluate C_{total} as a function of P_o, the value of λ should be swept.

It is worth mentioning that the data rate values obtained using (6) correspond to an ideal case where the only impairments considered are channel attenuation, crosstalk, and white Gaussian noise. Other impairments such as jitter, residual ISI, or quantization noise are not included. To include these impairments, we need to modify the SNR(f) formula, assuming a specific link architecture and a specific modulation scheme. This exercise is done for the cases of DMT and baseband in Sections III and IV.

C. DISCRETE MULTI-TONE (DMT) MODULATION

One method to reach capacity is by dividing the frequency band $\mathcal{B}$ into small sub-channels of width Δf. Through each sub-channel, the amount of transmit power is determined from the optimization solution made for (6) and (7). Knowing the optimum power spectral density $S_x(f)$, it is possible to define SNR(f) and the bit loading $b(f)$ of each sub-channel.

$$b(f) = \log_2\left(1 + \frac{SNR(f)}{\Gamma}\right) \tag{10}$$

One scheme suitable for this approach is DMT modulation, where the power and the number of bits transmitted in each sub-carrier are optimized towards maximizing the data rate.

A simplified block diagram of a DMT link is shown in Fig. 2, where QAM symbols form the complex amplitudes of sinusoids at different frequency bins. These complex amplitudes are then recovered at the receiver through a Fast Fourier Transform. In addition, the inclusion of cyclic prefix (CP), which appends the last portion of a given DMT block of symbols to its start, sets the input-output relation of the channel as circular convolution [13]. In this way, the addition of an IFFT block in the transmitter and FFT block in the receiver creates a communication link with N independent AWGN sub-channels (bins), each with input $X[l]$ and output $Y[l]$ related by:

$$Y[l] = X[l]H_C[l] + N[l] + \bar{X}[l]H_{XT}[l] \quad l = 1, 2, \ldots, N \tag{11}$$

In (11), the first term is the input multiplied by a complex number $H_C[l] = H_C(l\Delta f)$. To recover the transmit symbols,

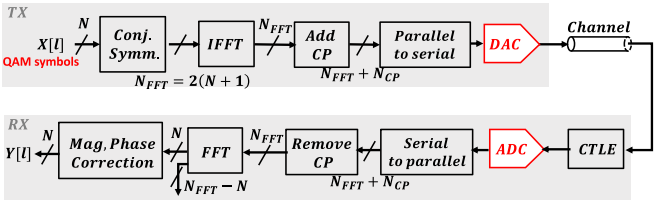

FIGURE 2. Simplified DMT link.

it is required the use of a magnitude and phase correction equalizer in each bin. The second term of (11) is the noise in the l-th sub-channel, and is given by $N[l] = \frac{N_o}{2}$. The third term in (11) represents an aggressor signal $\bar{X}[l]$ multiplied by the crosstalk transfer function in the l-th sub-channel, which can be written as $H_{XT}[l] = H_{XT}(l\Delta f)$.

"Bit and power loading" is the process of determining the number of bits per symbol and energy that is sent through each sub-channel. As the number of bits in each sub-band must be an integer, one approach is to round the optimal solution produced in (10) to the nearest integer value. However, this approach is not optimal. Instead, the optimal solution can be found by a bit loading algorithm, for example, Levin-Campello (LC) [14], [15], which is based on the concept of efficient bit distribution. To apply LC, we rely on two concepts:

- The minimum energy $\mathcal{E}_x(b, l)$ that is required to sustain b bits per transmission:

$$\mathcal{E}_x(b, l) = \frac{\Gamma\left(2^b - 1\right)\frac{N_o}{2}}{\max\{|H_C[l]|^2 - \Gamma\left(2^b - 1\right)|H_{XT}[l]|^2, 0\}} \tag{12}$$

- The incremental energy $\Delta\mathcal{E}_x(b, l)$, which is the energy required to increment the l-th bit load from b to $b+1$ bits:

$$\Delta\mathcal{E}_x(b, l) \triangleq \mathcal{E}_x(b+1, l) - \mathcal{E}_x(b, l) \tag{13}$$

An efficient bit distribution allocates bits and energy to the sub-carriers that requires less incremental energy. A flowchart, based on the LC implementation reported in [14], is illustrated in Fig. 3. The results of the LC algorithm are the vectors b and $\mathcal{E}_x$ with the bit load and energy per dimension of each bin. After the bit loading is applied, the achievable data rate is given by:

$$R = \frac{f_s}{N_{FFT} + N_{CP}} \sum_{l=1}^{N} b_l \tag{14}$$

where $f_s = 1/T$ is the data converter sampling rate, N_{FFT} is the size of the FFT/IFFT block and N_{CP} is the cyclic prefix size.

D. BASEBAND MODULATION

For a baseband system, the capacity calculation requires the analysis of the system in Fig. 1 with $T \neq 0$. This analysis, explained in [16], starts with a conversion from continuous to discrete-time. The immediate effect is that all transfer functions and power spectral densities are mapped

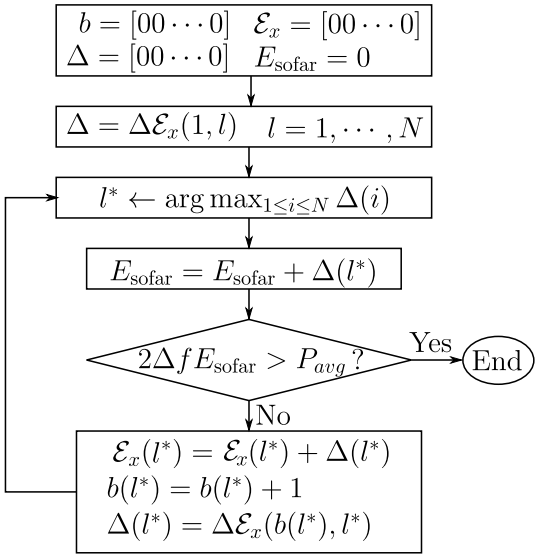

FIGURE 3. Levin-Campello algorithm.

to folded spectra. For example, the channel function $H_C(f)$ is mapped to:

$$\begin{aligned}\tilde{H_C}(f) = &\quad \tfrac{1}{T}\sum_{m=-\infty}^{\infty} H_C\big(f+\tfrac{m}{T}\big)\\ &\approx \tfrac{1}{T}\Big(H_C(f) + H_C\Big(\tfrac{1}{T}-f\Big)\Big)\end{aligned} \tag{15}$$

This approximation is valid for frequencies between 0 and $\frac{1}{2T}$ if spectrum aliasing is minimal. As a consequence, the achievable rate can be estimated with:

$$R(T) = \int_0^{\frac{1}{2T}} \log_2\left(1 + \frac{\text{SNR}^*(f)}{\Gamma}\right) df \tag{16}$$

where the SNR at the sampling point can be approximated by:

$$\text{SNR}^*(f) \approx \text{SNR}(f) + \text{SNR}\left(\frac{1}{T} - f\right) \tag{17}$$

Here, the optimization of the transmitter spectrum to maximize (16) is similar to the one performed for (6).

An interesting result reported by [17], [18] shows that a baseband system including a feed-forward equalizer and decision feedback equalizer, both optimized for minimum mean squared error, is, in theory, able to achieve the capacity of the channel. Under these conditions, the SNR at the slicer is referred to as Salz SNR, and is related to the achievable rate $R(T)$ by:

$$\text{SNR}_{\text{Salz}} = 2^{2TR(T)|_{\Gamma=1}} - 1 \tag{18}$$

Salz SNR can be thought of as an equivalent fixed SNR across the bandwidth $1/2T$ that results in the same data rate accommodated by SNR(f). Salz SNR has been used in the industry as a tool to evaluate communication links [19], [20] in the early design stage. The evaluation is done by comparing Salz SNR against the SNR for specific PAM-M modulation and BER requirements. An important point explained by Dong *et al.* [20] is that different impairments such as timing jitter or residual ISI, have not been included in Salz SNR analysis. To correct for an optimistic Salz SNR we must include an implementation penalty, usually in the order of 3dB to 5dB.

E. CAPACITY ANALYSIS VERSUS TIME DOMAIN SIMULATION

So far, we have described statistical-based analysis methods based on the concept of Salz SNR for PAM-M and bit loading for DMT. These methods are useful in finding quick estimates of the achievable data rate before the implementation of any time-domain model. However, we note that these methods are not intended to replace time-domain simulations, whereby important metrics such as horizontal/vertical eye openings can be extracted from time-domain models. In addition, a time-based simulation could include the effects of other impairments that may be challenging to include in a statistical-based analysis method.

III. MAXIMUM ACHIEVABLE RATE FOR DMT

A practical implementation of a DMT link is shown in Fig. 4(a). In this system, a conjugate symmetry block is added before the IFFT to obtain real-valued outputs. As the sub-channel at DC is usually not used, the size of the IFFT/FFT block is related to the number of available subcarriers by $N_{FFT} = 2(N+1)$. The number of non-zero pre and post-cursor ISI at the receiver when a single pulse is sent by the DAC determines the cyclic prefix size. Although fundamentally a CTLE is not required in DMT, its usage reduces the requirement on the CP size and its overhead on the data rate. Moreover, in general, the CTLE optimum parameters for DMT are different to those for baseband.

The bit loading procedure presented in Section II requires the inclusion of several impairments to evaluate the achievable data rate realistically. In this section, we describe how to improve the SNR(f) model, including the effect of jitter, residual ISI, data converter resolution, and clipping at the transmitter.

With this set of impairments, SNR(f) takes the form:

$$\begin{aligned}\text{SNR}(f) = \frac{S_x(f)\left|\bar{H}_C(f)\right|^2}{S_x(f)\left|\bar{H}_{XT}(f)\right|^2 + S_n(f) + S_{jit}(f) + \\ + S_{resISI}(f) + S_q(f) + S_{clip}(f)},\end{aligned} \tag{19}$$

where $S_{jit}(f)$, $S_{resISI}(f)$, $S_q(f)$, and $S_{clip}(f)$ represent the power spectral density of the noise created by sampling clock jitter, residual ISI, quantization noise and clipping, respectively. The analysis to obtain the parameters in (19) is described as follows. It should be noted that the study of clock and data recovery (CDR) for DMT and its comparison against the CDR for baseband signaling is not included in this work.

A. NOISE AND CROSSTALK

In the system of Fig. 4(a), the CTLE shapes the transmitted signal, crosstalk, and noise. To include this effect, we define

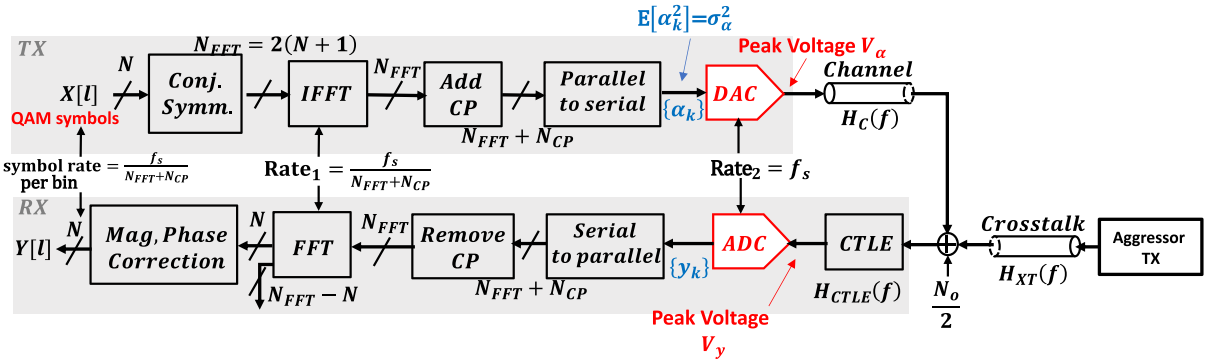

(a) DMT

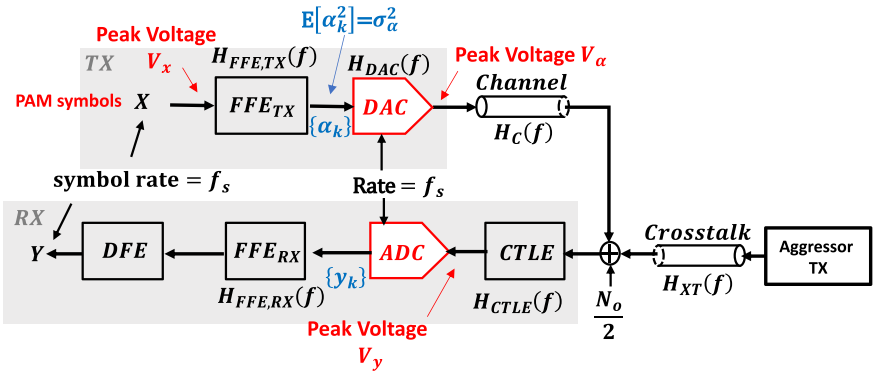

(b) Baseband

FIGURE 4. (a) DMT and (b) baseband PAM-M link architecture.

the combined channel-CTLE and crosstalk-CTLE transfer functions as:

$$\begin{aligned} |H_{C1}(f)| &\triangleq |H_C(f)||H_{CTLE}(f)| = \bar{H}_C(f) \\ |H_{XT1}(f)| &\triangleq |H_{XT}(f)||H_{CTLE}(f)| = \bar{H}_{XT}(f) \end{aligned} \tag{20}$$

$H_{C1}(f)$ is characterized by an impulse response $h_{C1}(t)$ and a sampled impulse response denoted by $h_m = h_{C1}(mT)$.

B. JITTER

For jitter analysis, we assume that the DAC input is composed of a sequence of symbols $\{\alpha_k\}$ running at a sampling rate $f_s = \frac{1}{T}$. Denoting the time uncertainty in the clock driving the DAC and ADC as ϵ_m^{TX} and ϵ_m^{RX} respectively, the noise signal at the ADC's output created by jitter at the transmitter and receiver by can be approximated by [21], [22]:

$$n_m^{TX} = \sum_k (\alpha_k - \alpha_{k-1})\epsilon_k^{TX} h_{m-k} \tag{21}$$

$$n_m^{RX} = \epsilon_m^{RX} \sum_k (\alpha_k - \alpha_{k-1}) h_{m-k} \tag{22}$$

where k is the index of the transmitted symbols, and m is the index of the symbols sampled by the ADC.

To be able to characterize the average power and the spectral behavior of n_m^{TX} and n_m^{RX}, we calculate the autocorrelation functions with:

$$\begin{aligned} R_{jit,TX}(w) &= E[n_m^{TX} n_{m+w}^{TX}] \\ &= 2\sigma_\alpha^2 E[(\epsilon_k^{TX})^2] R_h[w] \end{aligned} \tag{23}$$

$$\begin{aligned} R_{jit,RX}(w) &= E[n_m^{RX} n_{m+w}^{RX}] \\ &= \begin{cases} 2\sigma_\alpha^2 E[(n_m^{RX})^2](R_h[0] - R_h[1]) & \text{for } w = 0 \\ 0 & \text{for } w \neq 0 \end{cases} \end{aligned} \tag{24}$$

where σ_α^2 is the average power of $\{\alpha_k\}$ and $R_h[w] = \sum_k h_k h_{k+w}$.

An implicit assumption in this derivation is that both jitter and DAC inputs are uncorrelated, i.e., $E[\epsilon_k^{TX}\epsilon_{k^*}^{TX}] = E[\epsilon_k^{RX}\epsilon_{k^*}^{RX}] = E[\alpha_k \alpha_{k^*}] = 0$ for $k \neq k^*$. Moreover, it is possible to observe that n_m^{TX} and n_m^{RX} are stationary processes (independent of m), and their power spectral densities are respectively:

$$S_{jit,TX}(f) = 2\sigma_\alpha^2 E[(\epsilon_k^{TX})^2]|H_{C1}(f)|^2/T \tag{25}$$

$$S_{jit,RX}(f) = 2\sigma_\alpha^2 E[(\epsilon_k^{RX})^2](R_h[0] - R_h[1])/T \tag{26}$$

It is worth mentioning that the assumption of uncorrelated jitter (white spectrum jitter) is not always valid as the jitter spectrum depends on the oscillator noise profile and PLL/CDR transfer function. However, we assume uncorrelated jitter in this article to simplify the analysis and expressions.

C. RESIDUAL ISI: CYCLIC PREFIX SIZE

For this analysis, we denote by L_{SPR} the number of samples in the single pulse response of $H_{C1}(f)$. The cyclic prefix size is chosen to be $N_{CP} \geq L_{SPR} - 1$. However, if the single pulse response duration is long, it is not necessary to adhere to this inequality. A proper N_{CP} needs to maintain the noise power associated with insufficient CP size low, such that the performance is maintained.

The analysis done by [23], [24] shows that the selection of insufficient cyclic prefix size destroys the circular convolution relation from the input and output of the channel and creates interference within the DMT symbol block (also referred to as inter-carrier interference ICI) and interference caused by the previous DMT frame (which can be seen as ISI). Both sources of interference have the same average power in the l-th sub-carrier, given by:

$$P_{ISI}(l) \approx P_{ICI}(l) = \sigma_\alpha^2 \sum_{v=N_{CP}+1}^{L_{SPR}-1} |H_v(l)|^2 \tag{27}$$

where σ_α^2 is the average power of the transmitted signal, and $H_v(l)$ is the DFT of the tail samples of h_m that are not covered by the CP:

$$H_v(l) \triangleq \sum_{m=v}^{L_{SPR}-1} h_m e^{-j2\pi ml/N} \tag{28}$$

To be treated as a power spectral density, (27) must be normalized by the sub-carrier bandwidth Δf.

$$S_{resISI}(f)|_{f=l\Delta f} = 2\frac{P_{ISI}(l)}{\Delta_f} \tag{29}$$

It is worth mentioning that although the energy of ISI and ICI is similar, their timing is different, requiring the use of DFE to remove ISI and cross-DFE (XDFE), i.e., a DFE that uses the information of other bins, to remove ICI [25]. Nevertheless, statistical modeling of these impairments does not rely on their timing.

D. DAC AND ADC QUANTIZATION NOISE

Suppose a given DAC and ADC both with resolution N_{bit}. If the DAC's peak to peak output range and the ADC's peak to peak input range are limited to $2V_\alpha$ and $2V_y$, respectively, their quantization steps are defined as $\Delta_{DAC} = \frac{2V_a}{2^{N_{bit}}}$ and $\Delta_{ADC} = \frac{2V_y}{2^{N_{bit}}}$.

A common assumption for data converter quantization noise is that any possible error is uniformly distributed in the interval of width Δ_{DAC} or Δ_{ADC}. Moreover, assuming that quantization errors are independent and identically distributed, the power spectral density is white over the frequency range from $-f_s/2$ to $f_s/2$. As the DAC quantization noise propagates through the channel, its spectral density is shaped by the channel frequency response. With these considerations, the power spectral density for quantization noise created by DAC and ADC is approximated as:

$$\begin{aligned} S_{q,DAC}(f) &= \tfrac{\Delta_{DAC}^2}{12f_s}|H_{C1}(f)|^2 \\ S_{q,ADC}(f) &= \tfrac{\Delta_{ADC}^2}{12f_s}. \end{aligned} \tag{30}$$

E. CLIPPING AT TX

When the number of sub-channels is high, the sum of all their respective tones could potentially create a peak amplitude that is larger that the DAC's output range, resulting in some clipping. To evaluate an acceptable level of clipping, [26] calculates the average power of the clipped portion of the signal as:

$$P_{clip} = \sigma_\alpha^2 \left[(1+\mu^2)\,\mathrm{erfc}\left(\frac{\mu}{\sqrt{2}}\right) - \mu\sqrt{\frac{2}{\pi}}\exp\left(-\frac{\mu^2}{2}\right)\right] \tag{31}$$

where the parameter $\mu \triangleq \frac{V_a}{\sigma_\alpha}$ is referred to as Clipping Factor.

As a first approximation, the clipping noise can be assumed as white over $-f_s/2$ to $f_s/2$. Since the TX clipping noise is shaped by the channel, its power spectral density can be approximated by:

$$S_{clip}(f) = \frac{P_{clip}}{f_s}|H_{C1}(f)|^2 \tag{32}$$

It is worth mentioning that this approach is an approximation that ignores possible non-linearities at the transmitter that may cause additional ISI or ICI. In addition, we do not consider the interaction between quantization noise and clipping, as reported in [27]. Time-domain simulations can be considered to include these effects at a later stage of the design.

IV. MAXIMUM ACHIEVABLE RATE FOR BASEBAND MODULATION

A practical implementation of a baseband PAM-M link is shown in Fig. 4(b). In this system, the use of equalization employing CTLE, feed-forward equalizer (FFE) at the transmitter and the receiver, and decision feedback equalizer (DFE) help to reduce ISI. For this analysis, we assume the DAC at the transmitter to interpolate the discrete input sequence with a zero-order hold, which introduces a frequency response $H_{DAC}(f) = \mathrm{sinc}(fT)$. In addition, we consider the power spectral density of the discrete-time sequence X given by:

$$S_x(f) = \frac{V_x^2}{3}\left(\frac{M+1}{M-1}\right)T, \tag{33}$$

where V_x is the peak voltage swing of the PAM-M symbols sequence X. To be able to calculate Salz SNR, the effect of impairments such as quantization noise, jitter, and residual ISI should be considered. With this set of impairments, the SNR(f) takes the same form as (19), but some of the terms are different, as described below.

A. NOISE AND CROSSTALK

Noise and Crosstalk are treated in a similar way as DMT by defining the combined channel-equalizer and crosstalk-equalizer transfer functions as:

$$\bar{H}_C(f) \triangleq |H_{FFE,TX}(f)||H_{DAC}(f)||H_C(f)| \quad (34)$$
$$|H_{CTLE}(f)||H_{FFE,RX}(f)| \quad (35)$$
$$\bar{H}_{XT}(f) \triangleq |H_{FFE,TX}(f)||H_{DAC}(f)||H_{XT}(f)| \quad (36)$$
$$|H_{CTLE}(f)||H_{FFE,RX}(f)|. \quad (37)$$

B. JITTER

Consider the transmission of a sequence of PAM-M symbols x_k with a peak to peak signal swing $2V_x$, corresponding to an average power per symbol $\sigma_x^2 = \frac{M+1}{3(M-1)}V_x^2$. This sequence usually goes through a transmitter FFE to produce a sequence $\alpha_k = C_0x_k + C_1x_{k-1} + \cdots + C_nx_{k-n}$, where C_0 to C_n are the FFE coefficients. After the transmitter FFE, the voltage swing is $V_\alpha = (|C_0| + |C_1| + \cdots + |C_n|)V_x$ and the average power is $\sigma_\alpha^2 = (C_0^2 + C_1^2 + \cdots + C_n^2)\sigma_x^2$.

For the jitter analysis, it is possible to use a similar derivation as the one used to derive (25) and (26), with the main difference being the DAC transmitted sequence is now correlated due to the FFE. Assuming uncorrelated jitter, the autocorrelation functions of the TX and RX jitter induced noise after the ADC are:

$$R_{jit,TX}(w) = \Big(2\sigma_\alpha^2 - 2R_\alpha[-1]\Big)E[(\epsilon_k^{TX})^2]R_h[w] \quad (38)$$
$$R_{jit,RX}(w) = E[(n_m^{RX})^2]\sum_{\tau=-\infty}^{\infty}\{2R_\alpha[\tau] - R_\alpha[\tau-1] \quad (39)$$
$$-R_\alpha[\tau+1]\}R_h[\tau] \quad (40)$$

where the correlation of α_k is calculated with $R_\alpha[\tau] = (C_0C_{|\tau|} + C_1C_{|\tau|+1} + \cdots + C_{n-|\tau|}C_n)\sigma_\alpha^2$.

The spectral densities of the TX and RX jitter induced noise before the receiver FFE are given by:

$$S_{jit,TX}(f) = \Big(2\sigma_\alpha^2 - 2R_\alpha[-1]\Big)E[(\epsilon_k^{TX})^2]|H_{C1}(f)|^2/T \quad (41)$$
$$S_{jit,RX}(f) = \frac{1}{T}E[(n_m^{RX})^2]\sum_{\tau=-\infty}^{\infty}\{2R_\alpha[\tau] - R_\alpha[\tau-1] \quad (42)$$
$$-R_\alpha[\tau+1]\}R_h[\tau]. \quad (43)$$

C. RESIDUAL ISI

After equalizing the channel, it is possible to decompose the sampled pulse response in two components, namely the ISI-free response h_{noISI} and the residual ISI response h_{resISI} (Fig. 5):

$$h_{EQ} = h_{noISI} + h_{resISI} \quad (44)$$

Taking Fourier transform of both sides, we can evaluate the transfer function of the residual ISI term as:

$$H_{resISI}(f) = H_{EQ}(f) - 1 \quad (45)$$

With this transfer function, it is possible to evaluate the residual ISI power spectral density as:

$$S_{resISI}(f) = S_x(f)|H_{resISI}(f)|^2. \quad (46)$$

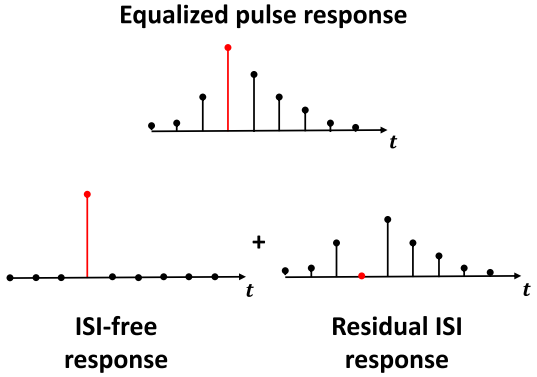

FIGURE 5. Decomposition of equalized pulse response.

D. QUANTIZATION NOISE AND CLIPPING

For DAC and ADC quantization noise, the power spectral densities are shaped by the receiver FFE.

$$S_{q,DAC}(f) = \frac{\Delta_{DAC}^2}{12f_s}|H_{C1}(f)|^2|H_{FFE,RX}(f)|^2 \quad (47)$$
$$S_{q,ADC}(f) = \frac{\Delta_{ADC}^2}{12f_s}|H_{FFE,RX}(f)|^2 \quad (48)$$

The de-emphasis operation applied in the TX ensures amplitudes in the DAC output never exceed V_α, hence for baseband transmission, clipping can be neglected.

E. MAXIMUM RATE CHARACTERIZATION

With the updated model of SNR(f), it is possible to characterize the maximum achievable rate as a function of the full-scale voltage using an iterative approach based on Salz SNR.

The characterization method is shown in Fig. 6 and is described as follows. Given a modulation order M, an initial baud rate $BR_1 = 1/T_1$ and a DAC full-scale voltage V_α, we can initialize the data rate as $R = \frac{\log_2(M)}{T_1}$ and calculate SNR(f) and Salz SNR using equations (18) and (19), respectively. This SNR is compared with the required SNR for a target symbol error rate, which is known to be [14]:

$$SNR_{req} = \left(\frac{M^2-1}{3}\right)\left(Q^{-1}\left(\frac{M\cdot P_e}{2(M-1)}\right)\right)^2 \quad (49)$$

Based on this comparison, it can be decided whether the baud rate should be increased or decreased for the next iteration. The iteration stops when the difference between Salz SNR and the required SNR is γ_m, which represents an implementation margin. This margin is ideally 1, but can be assumed slightly higher, such as 1.25, to improve convergence. Finally, this process can be repeated for different values of V_α.

V. SIMULATION RESULTS

As discussed so far, the maximum achievable data rate for a channel depends first and foremost on the channel characteristics, namely its insertion loss (frequency response), noise profiles, and crosstalk profiles. Once we pick a channel, then the maximum achievable rate will

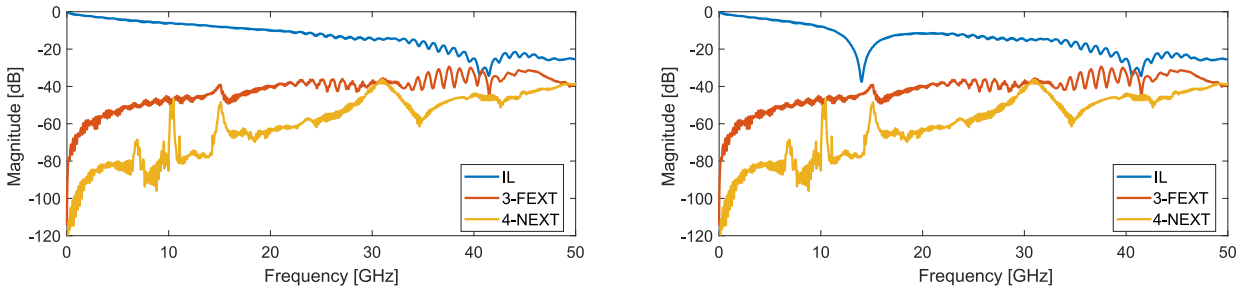

(a) Smooth channel (b) Notch channel

FIGURE 7. Insertion loss and crosstalk for (a) the smooth and (b) the notch channel.

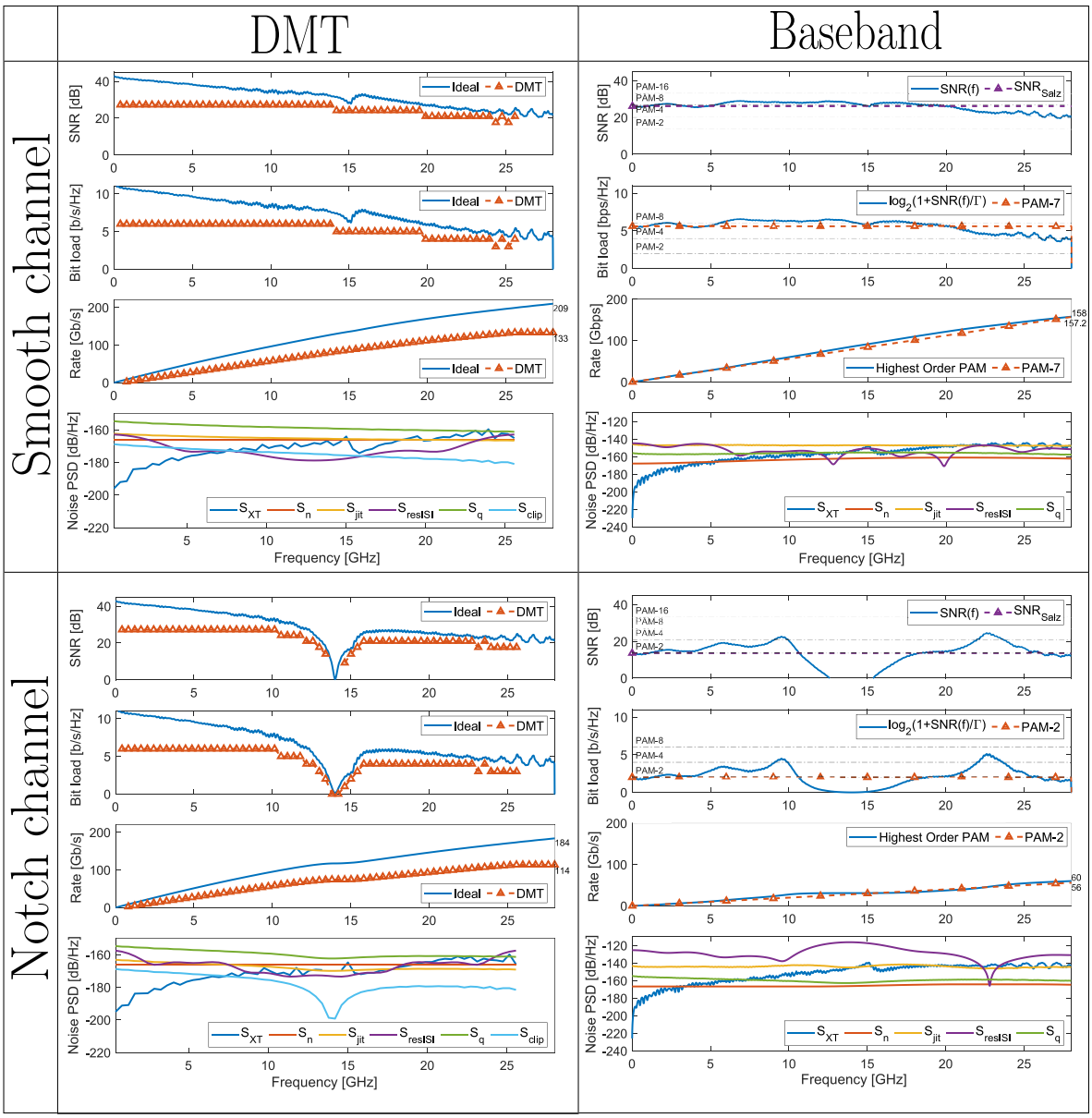

FIGURE 8. Simulation results for the smooth and notch channel for each of DMT and baseband signaling.

depend on the modulation scheme, its particular implementation, and the complexity we are ready to deploy in its implementation.

In this section, we simulate the maximum achievable data rates for two distinct channels: 1. a "smooth channel", which is publicly available through the IEEE 802.3 Ethernet

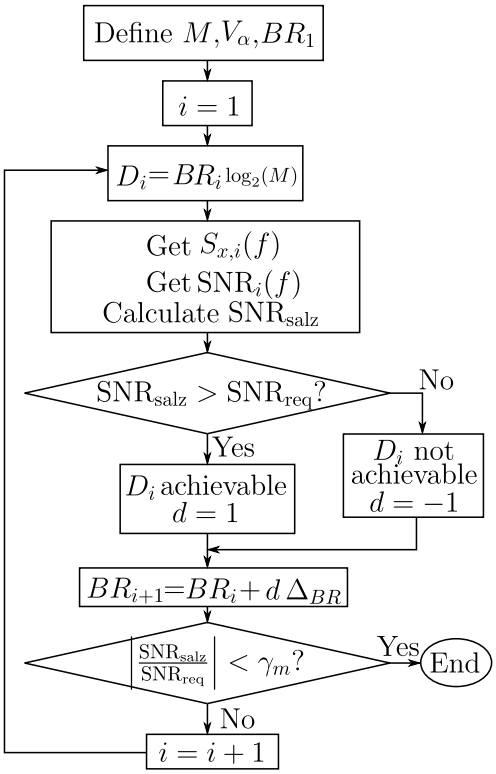

FIGURE 6. Baseband maximum achievable rate characterization method.

Working Group [29]. This channel, shown in Fig. 7(a), is specified with an insertion loss of −14dB at 28GHz, the Nyquist frequency for a PAM-4 system running at 112 Gb/s, and two specific crosstalk profiles. 2. a recreated "notch channel," shown in Fig. 7(b), which has the same crosstalk profile as the smooth channel, but its insertion loss exhibits a 30dB notch at 14GHz. Notches in channel response are not uncommon and can, for example, be created by impedance discontinuities due to vias, stubs, and connectors. An example of impedance discontinuity notch is demonstrated for multi-drop memory bus applications in [7]. Channels of this characteristic are known to be challenging to equalize with conventional baseband techniques.

For each of the DMT and Baseband signaling schemes, we choose the equalization parameters (CTLE in both modulations, FFE in baseband only) so as to maximize the data rate for that scheme. For DMT, we design the CTLE so as to limit the size of the cyclic prefix to 10. This is simply to avoid a significant data rate penalty.

For a fair comparison between the two signaling schemes, we have used the same design parameters for both signaling schemes wherever possible. A complete list of these parameters is shown in Table 1. In particular, both the DAC and the ADC use the same resolution (6 bits), same sampling rate (56GS/s), and same rms jitter (150fs).

Fig. 8 compares the DMT and the baseband signaling for the smooth and notch channels. The results of DMT for the smooth channel are presented in four plots:

TABLE 1. Simulation settings.

Component	Characteristics
Channel	14dB insertion loss at 28GHz with and without notch
$N_o/2$	5.2e-8 $\mathrm{V}^2/\mathrm{GHz}$
DAC	6 bits, $f_s \leq$ 56GS/s, TX swing: $2V_\alpha = 1$ $\mathrm{V_{pp\text{-}diff}}$, TX RJ: $\sigma_{\mathrm{jit}} = 150$ $\mathrm{fs_{rms}}$
ADC	6 bits, $f_s \leq$ 56GS/s, full-scale range $2V_y =$ 0.4 $\mathrm{V_{pp\text{-}diff}}$, sampling clock RJ: $\sigma_{\mathrm{jit}} = 150$ $\mathrm{fs_{rms}}$
CTLE	Transfer function with 1 variable pole, 1 variable zero, and 3 fixed poles at 30GHz [28]. Optimized to reduce residual ISI in pulse response for $T = 1/f_s$.
Symbol error rate (SER)	1e-6
FFT Size	128
CP size	10
FFE taps	3 at TX, 6 at RX

- The first plot shows the evaluation of SNR(f) for two particular cases: (a) the ideal SNR, assuming insertion loss, crosstalk and AWGN as the only impairments in the system; and (b) the SNR(f) for the DMT case including the set of impairments described in Section III.
- The second plot shows the bit load in bps/Hz for the ideal case and the DMT case. We observe that in the ideal scenario, constellations up to QAM-2^{11} are achievable. In the DMT case, constellations up to QAM-64 are achievable.
- The third plot shows the data rate that is obtained by integrating the bit load plots. The DMT signaling can accommodate a data rate up to 133Gb/s, whereas ideally we could have expected a data rate up to 209Gb/s.
- The fourth plot shows the spectral density of the noise signals created by the different impairments. Integration of these spectral densities allows us to identify the dominant impairment in the system. In this particular example, the dominant impairment is quantization noise, which contributes 2.8$\mathrm{mV_{rms}}$, followed by jitter and AWGN, which contribute 1.3$\mathrm{mV_{rms}}$ and 1.2$\mathrm{mV_{rms}}$, respectively.

The results of Baseband for the smooth channel are presented in four plots:

- The first plot shows the SNR(f) for the baseband case including the set of impairments described in Section IV. In addition, the evaluated Salz SNR is plotted and compared against the required SNR for different PAM modulation orders. In this case, the Salz SNR (26.21dB) is close to but slightly lower than the SNR required by PAM-8 (26.96dB). In fact, 26.21dB of Salz SNR can sustain a PAM-M modulation with no more than $M = 7.35$ levels. This is equivalent to state that $M = 7.35$ is the "Highest Order Achievable PAM". Under these circumstances, to meet the requirement of

SER=1e-6, it is necessary to reduce modulation order to PAM-7 if we impose a constrain of an integer number of bits per symbol.

- The second plot shows the bit load, in bps/Hz, as a function of frequency using $\log_2(1 + \frac{\text{SNR}}{\Gamma})$. We also show the bit load for PAM-7 modulation, which is 5.6 bps/Hz.
- The third plot, obtained by integrating the bit load plots, indicates that the achievable data rate is 157.2Gb/s for PAM-7 whereas, ideally, it could be 158Gb/s if PAM-M with $M = 7.35$ were implementable.
- The fourth plot shows the spectral density of the noise signals created by the different impairments. Integration of these spectral densities allows us to identify the dominant impairment in the system. In this particular example, the dominant impairments are jitter, residual ISI and crosstalk, with contributions to the total noise of 11.8mV$_{\text{rms}}$, 7.9mV$_{\text{rms}}$, and 7.6mV$_{\text{rms}}$, respectively.

The results of DMT for the notch channel are presented similarly in Fig. 8. The bit rates for the ideal and DMT cases are 184Gb/s and 114Gb/s, respectively. The integration of the noise spectral densities allows us to identify that the dominant impairments are quantization noise, AWGN, and jitter, with contributions of 2.59mV$_{\text{rms}}$, 1.13mV$_{\text{rms}}$ and 0.99mV$_{\text{rms}}$, respectively. For the baseband case in the notch channel, the Salz SNR reduces to 13.56dB, slightly higher than 13.54dB of SNR required for PAM-2 with SER=1e-6. Under these conditions, the data rate reduces to 56Gb/s. The integration of the noise spectral densities allows us to identify that the dominant impairment is residual ISI with 147mV$_{\text{rms}}$, followed by jitter with 15.1mV$_{\text{rms}}$.

Although the simulation results of Fig. 8 suggest that the DMT signaling may be superior to baseband signaling for the notch channel, the performance of DMT signaling scheme can be far more sensitive to design parameters, which may directly translate to design complexity. To complete this study, we compare the performance sensitivity of the two signaling schemes to each of ADC/DAC resolution, jitter, transmit signal swing, crosstalk, and residual ISI.

A. EFFECT OF DAC AND ADC RESOLUTION

Fig. 9 compares the performance of DMT and baseband signaling as a function of the DAC and ADC resolution. For the smooth channel, the DMT performance is very sensitive to the data converter resolution. In order to get comparable performance to PAM-8, 7 bits of resolution are required by DMT. In the case of baseband, the minimum resolution depends on the modulation order. For example, PAM-8 requires at least 6 bits of resolution, PAM-4 can tolerate a reduction down to 4 bits, and PAM-2 is unaffected by a resolution drop to 3 bits. DMT maintains its performance when we move from the Smooth Channel to the Notch Channel. In contrast, baseband signaling suffers a significant drop in the achievable data rate. This is expected as the notch can be avoided by DMT but causes major ISI, not removable by CTLE, for the baseband case.

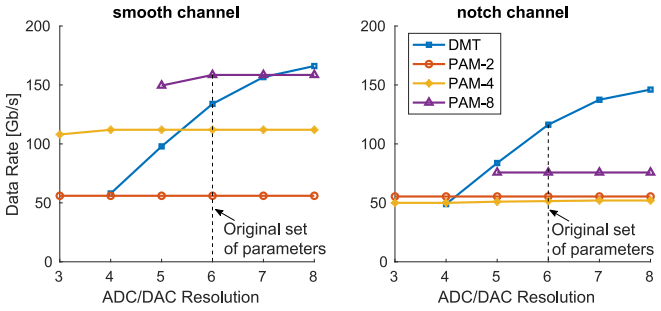

FIGURE 9. Achievable rate vs. ADC/DAC resolution for DMT and baseband. In this simulation, σ_{jit} = 150 fs$_{rms}$, 1 V$_{\text{pp-diff}}$ DAC swing, and both channels are used.

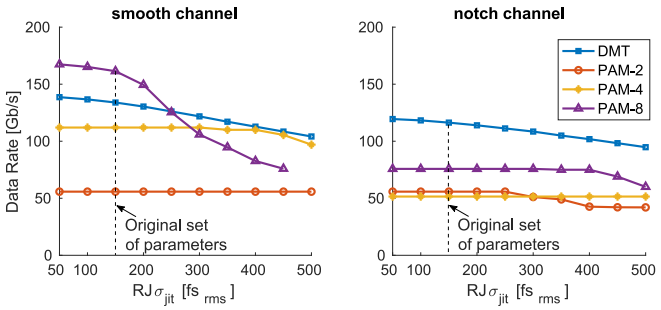

FIGURE 10. Achievable rate vs. σ_{jit}. In this simulation, 1 V$_{\text{pp-diff}}$ DAC swing, N_{bit} = 6, and both channels are used.

B. EFFECT OF JITTER

To compare the impact of random jitter on the achievable data rate, we have swept σ_{jit} from 50 to 500 fs$_{rms}$ for both channels. The results are shown in Fig. 10. For the smooth channel, PAM-8 data rate is the most sensitive to jitter, whereas DMT and PAM-4 exhibit similar degradations for σ_{jit} greater than 400fs$_{rms}$. For the notch channel, jitter does not show an impact on the achievable data rate because baseband link performance is limited by residual ISI. DMT shows a similar degradation for both the smooth and notch channels.

C. EFFECT OF TRANSMITTER SWING

Defining the transmitter output swing is a critical step in the system level definition of the link. A higher voltage swing increases the overall SNR, and consequently, the link may improve the data rate or the bit error rate for a given set of impairments. However, a higher voltage can impact reliability, power consumption, or linearity of the system.

Fig. 11 shows the performance of both DMT and baseband as a function of the transmitter voltage swing. The simulations are done for the smooth and notch channels. In the smooth channel, DMT is most sensitive to swing followed by PAM-8, while PAM-4 and PAM-2 data rates are unaffected by the swing. In the notch channel, the performance of baseband is not affected by the swing since it is already degraded severely by the notch. In contrast, the DMT performance continues to improve with the swing.

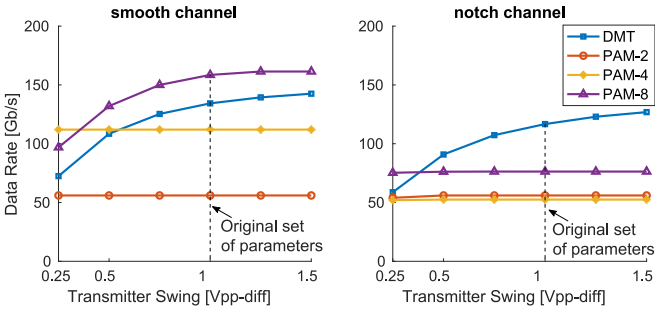

FIGURE 11. Achievable rate vs. transmitter peak to peak voltage for DMT and baseband. In this simulation, $N_{bit} = 6$, $\sigma_{jit} = 150$ fs$_{rms}$, and both channels are used.

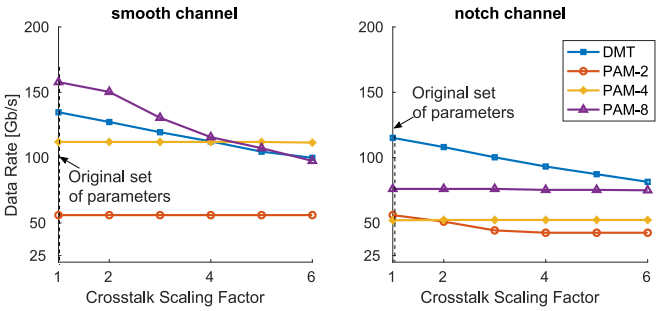

FIGURE 12. Data rate vs. crosstalk for DMT and baseband. In this simulation, $N_{bit} = 6$, $\sigma_{jit} = 150$ fs$_{rms}$, 1 V$_{pp\text{-}diff}$ DAC swing, and both channels are used.

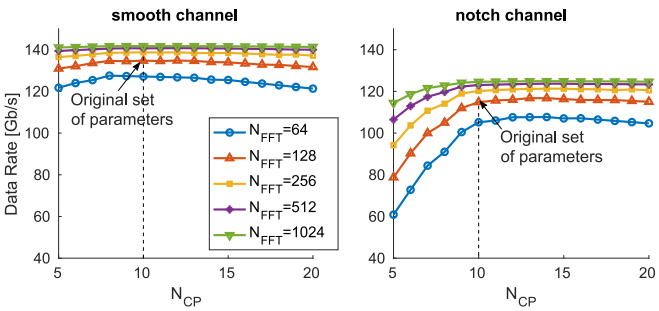

FIGURE 13. DMT achievable rate vs. CP and FFT size. In this simulation, $N_{bit} = 6$, $\sigma_{jit} = 150$ fs$_{rms}$, 1 V$_{pp\text{-}diff}$ DAC swing, and both channels are used.

D. EFFECT OF CROSSTALK

To evaluate the effect of crosstalk, we applied a scaling factor to the crosstalk transfer function and varied this parameter to observe the achievable data rate. Similar to the case of jitter, for the smooth channel, PAM-8 suffers more from crosstalk compared with other modulations, whereas the degradation in PAM-4 is similar to DMT. For the notch channel, while the performance of the baseband schemes that have already been limited by the notch do not show much sensitivity to crosstalk, the performance of DMT continues to be affected by increasing crosstalk. Naturally, at high crosstalk levels, baseband schemes start to be affected by crosstalk, starting with PAM-8.

E. EFFECT OF INCREASING COMPLEXITY

In the absence of an exact area and power estimate for each of baseband and DMT signaling, we resort to observing the impact on the data rate as a result of increasing the CP size and FFT size in DMT and of increasing the number of FFE taps in baseband. Although these are not the only parameters affecting the overall complexity, they are likely to be among the most impactful. Fig. 13 shows how the achievable rate for DMT changes with the CP size and N_{FFT}. We observe that a CP size of 10 is optimum for both the smooth and notch channels. Also, the data rate improves with the size of the FFT. However, for FFT values higher than 128, the improvement in data rate is not high enough to justify an increase in the size of the FFT block.

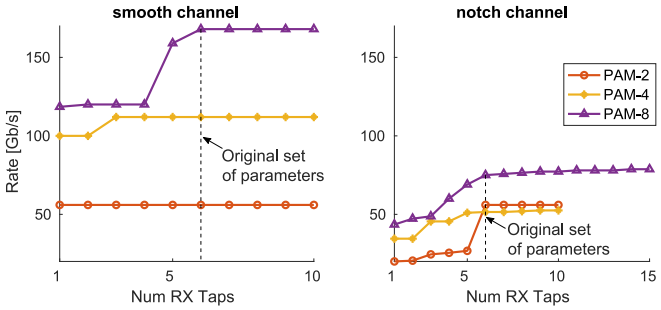

FIGURE 14. Baseband achievable rate vs. amount of taps in the RX FFE. In this simulation, $N_{bit} = 6$, $\sigma_{jit} = 150$ fs$_{rms}$, 1 V$_{pp\text{-}diff}$ DAC swing, 3 taps at the transmitter FFE, and both channels are used.

For the case of baseband, aside from the CTLE, the parameter which can be selected to increase the achievable data rate is the number of FFE taps. To evaluate this, for both channels, we sweep the number of taps in the receiver. Fig. 14 shows that increasing the number of taps does increase the data rate but only to a certain point, beyond which the data rate shows no increase with the number of taps.

Another aspect that needs to be considered in the complexity evaluation is the discrepancy between the channel model and the actual channel response and its impact on the link performance. At the design stage, an initial approach is to include a varying scaling factor in the channel insertion loss $|H_c(f)|$. In this way, it is possible to run bit-loading and obtain the range of achievable data rates. However, we also notice that further research is required to study the effect created by variations in the insertion loss's shape.

VI. CONCLUSION

In this article, we compared baseband against DMT to determine which signaling scheme can provide a higher data rate for the same channel. Given a set of constraints, namely the ADC/DAC resolution, rms of random jitter, transmitter signal swing, the thermal and the integrated crosstalk noise, we have shown that the DMT signaling can achieve a data rate of 133Gb/s and 114Gb/s for the smooth channel and the notch channel, respectively, whereas the baseband signaling can accommodate a higher data rate (157.2Gb/s) for the smooth channel but a substantially lower data rate (56Gb/s) for the notch channel. Given the smooth channel can be equalized easily to provide an effective flat frequency response explains why baseband signaling has an advantage in this case. On the other hand,

TABLE 2. A summary of data rate sensitivity of DMT and baseband signaling to each of the constraints.

Constraints		DMT Sensitivity	Baseband Sensitivity	Detailed Data
ADC/DAC Resolution		High	Medium for PAM-8 in smooth channel Very Low for others	Fig. 9
Random Jitter		Medium	High for PAM-8 in smooth channel Low for others	Fig. 10
Transmitter Swing		High	High for PAM-8 in smooth channel Very Low for others	Fig. 11
Crosstalk		Medium	Medium for PAM-8 in smooth channel Low for others	Fig. 12
Complexity	CP Size	High in notch channel Medium in smooth channel	N/A	Fig. 13
	FFT Size	High in notch channel Medium in smooth channel	N/A	Fig. 13
	RX FFE Taps	N/A	Medium (more in notch channel)	Fig. 14

it is difficult for the baseband signaling to provide effective equalization when there is a notch in the channel. This explains why DMT signaling, which can effectively bypass the notch, has an advantage over baseband signaling in this case. To find out how robust the performance of each of the signaling scheme is to the constraints, we have swept these constraints, one at a time, and simulated their corresponding maximum achievable rates. Table 2 summarizes these results, suggesting overall a higher sensitivity of DMT signaling to design parameters compared with baseband signaling.

ACKNOWLEDGMENT

The authors thank the anonymous reviewers of this article for their valuable feedback on the first draft of this article. They also thank Huawei Canada for their expertise and assistance throughout the course of this research. Access to CAD tools was provided by CMC Microsystems.

REFERENCES

[1] J. Im *et al.*, "6.1 A 112Gb/s PAM-4 long-reach wireline transceiver using a 36-way time-interleaved SAR-ADC and inverter-based RX analog front-end in 7nm FinFET," in *Proc. IEEE Int. Solid-State Circuits Conf. (ISSCC)*, 2020, pp. 116–118.

[2] T. Ali *et al.*, "6.2 A 460mW 112Gb/s DSP-based transceiver with 38dB loss compensation for next-generation data centers in 7nm FinFET technology," in *Proc. IEEE Int. Solid-State Circuits Conf. (ISSCC)*, 2020, pp. 118–120.

[3] C. Menolfi *et al.*, "A 112Gb/S 2.6pJ/b 8-tap FFE PAM-4 SST TX in 14nm CMOS," in *Proc. IEEE Int. Solid-State Circuits Conf. (ISSCC)*, 2018, pp. 104–106.

[4] A. Cevrero *et al.*, "6.1 A 100Gb/s 1.1pJ/b PAM-4 RX with dual-mode 1-tap PAM-4/3-tap NRZ speculative DFE in 14nm CMOS FinFET," in *Proc. IEEE Int. Solid-State Circuits Conf. (ISSCC)*, Feb. 2019, pp. 112–114.

[5] G. Kim *et al.*, "30.2 A 161mW 56Gb/s ADC-based discrete multi-tone wireline receiver data-path in 14nm FinFET," in *Proc. IEEE Int. Solid-State Circuits Conf. (ISSCC)*, Feb. 2019, pp. 476–478.

[6] V. Stojanovic, A. Amirkhany, and M. A. Horowitz, "Optimal linear precoding with theoretical and practical data rates in high-speed serial-link backplane communication," in *Proc. IEEE Int. Conf. Commun.*, vol. 5, Jun. 2004, pp. 2799–2806.

[7] A. Amirkhany, "Multi-carrier signaling for high-speed electrical links," Ph.D. dissertation, Dept. Electric. Eng., Stanford Univ., Stanford, CA, USA, 2008.

[8] C. E. Shannon, "A mathematical theory of communication," *Bell System Tech. J.*, vol. 27, pp. 379–423, Jul. 1948.

[9] T. M. Cover and J. A. Thomas, *Elements of Information Theory*. Hoboken, NJ, USA: Wiley-Intersci., 2006.

[10] N. Al-Dhahir and J. M. Cioffi, "Symbol rate optimization for the MMSE-DFE on bandlimited dispersive channels," *Digit. Signal Process.*, vol. 6, no. 2, pp. 73– 95, 1996. [Online]. Available: http://www.sciencedirect.com/science/article/pii/S1051200496900093

[11] A. Sanders, M. Resso, and J. D'Ambrosia, "Channel compliance testing utilizing novel statistical eye methodology," in *Proc. DesignCon*, 2004, pp. 1–25.

[12] I. Kalet and S. Shamai, "On the capacity of a twisted-wire pair: Gaussian model," *IEEE Trans. Commun.*, vol. 38, no. 3, pp. 379–383, Mar. 1990.

[13] B. P. Lathi and Z. Ding, *Modern Digital and Analog Communication Systems*. Oxford, U.K.: Oxford Univ. Press, 2009.

[14] J. M. Cioffi, *Lecture Notes for Advanced Digital Communication: Multi-Channel Modulation*. Stanford, CA, USA: Stanford Univ., 1997. [Online]. Available: https://cioffi-group.stanford.edu/doc/book/chap4.pdf

[15] J. Campello, "Practical bit loading for DMT," in *Proc. IEEE Int. Conf. Commun.*, vol. 2, Jun. 1999, pp. 801–805.

[16] G. Ungerboeck, "Achievable bit rates and choice of modulation rate for 10GBASE-T," presented at the IEEE P802.3an Task Force Meeting, Long Beach, CA, USA, May 2004. [Online]. Available: https://www.ieee802.org/3/an/public/may04/ungerboeck_1_0504.pdf

[17] J. M. Cioffi, G. P. Dudevoir, M. V. Eyuboglu, and G. D. Forney, "MMSE decision-feedback equalizers and coding. I. Equalization results," *IEEE Trans. Commun.*, vol. 43, no. 10, pp. 2582–2594, Oct. 1995.

[18] J. M. Cioffi, G. P. Dudevoir, M. V. Eyuboglu, and G. D. Forney, "MMSE decision-feedback equalizers and coding. II. coding results," *IEEE Trans. Commun.*, vol. 43, no. 10, pp. 2595–2604, Oct. 1995.

[19] H. Wong, X. Dong, and F. Tremblay, "Salz SNR modification for high speed serial link system performance estimation," in *Proc. DesignCon*, 2012, pp. 1061–1111.

[20] X. Dong *et al.*, "112G electrical system performance study based on an improved salz SNR methodology," in *Proc. DesignCon*, 2018, pp. 1–25.

[21] J. Caroselli and C. Liu, "An analytic system model for high speed interconnects and its application to the specification of signaling and equalization architectures for 10 Gbps backplane communication," in *Proc. DesignCon*, 2006, pp. 1464–1484.

[22] K. S. Oh *et al.*, "Accurate system voltage and timing margin simulation in high-speed I/O system designs," *IEEE Trans. Adv. Packag.*, vol. 31, no. 4, pp. 722–730, Nov. 2008.

[23] W. Henkel, G. Taubock, P. Odling, P. O. Borjesson, and N. Petersson, "The cyclic prefix of OFDM/DMT—An analysis," in *Proc. Int. Zurich Seminar Broadband Commun. Access Transm. Netw.*, Feb. 2002, p. 22.

[24] D. J. F. Barros and J. M. Kahn, "Optimized dispersion compensation using orthogonal frequency-division multiplexing," *J. Lightw. Technol.*, vol. 26, no. 16, pp. 2889–2898, Aug. 15, 2008.
[25] J. Zhu, W. Ser, and A. Nehorai, "Channel equalization for DMT with insufficient cyclic prefix," in *Proc. Conf. Rec. 34th Asilomar Signals Syst. Comput.*, vol. 2, 2000, pp. 951–955.
[26] D. J. G. Mestdagh, P. Spruyt, and B. Biran, "Analysis of clipping effect in DMT-based ADSL systems," in *Proc. ICC/SUPERCOMM Int. Conf. Commun.*, vol. 1, May 1994, pp. 293–300.
[27] D. Dardari, "Joint clip and quantization effects characterization in OFDM receivers," *IEEE Trans. Circuits Syst. I, Reg. Papers*, vol. 53, no. 8, pp. 1741–1748, Aug. 2006.
[28] H. Shakiba *et al.*, "Methodology for performance comparison of center and edge sampling in serial links," *Signal Integr. J.*, Jul. 2019. [Online]. Available: https://www.signalintegrityjournal.com/articles/1293-methodology-for-performance-comparison-of-center-and-edge-sampling-in-serial-links
[29] R. Mellitz, "100 GEL C2M flyover host files: Tp0 to Tp2, with and without manufacturing variations, for losses 9, 10, 11, 12, 13, and 14 dB," presented at the IEEE 802.3 100GEL Study Group, Pittsburg, PA, USA, May 2018. [Online]. Available: https://www.ieee802.org/3/ck/public/18_05/mellitz_3ck_02_0518.pdf

JHOAN SALINAS (Graduate Student Member, IEEE) received the B.S.E.E. degree (*cum laude*) from the Universidad Industrial de Santander, Bucaramanga, Colombia, in 2009, and the M.Sc. degree from the Instituto Nacional de Astrofisica, Optica y Electronica, Puebla, Mexico, in 2012. He is currently pursuing the Ph.D. degree with the Department of Electrical and Computer Engineering, University of Toronto, Canada. His research interests are the estimation of the maximum data rate that can be transmitted through a given wired channel, and the design of novel architectures for next-generation baseband PAM-M, and multiple tone wireline systems.

JEREMY COSSON-MARTIN (Student Member, IEEE) received the B.A.Sc. degree in electrical engineering from Queen's University, Kingston, ON, Canada, in spring of 2018. In fall of 2018, he began the M.A.Sc program with the University of Toronto, ON, Canada, under the supervision of Professor Ali Sheikholeslami. In summer of 2018, he joined Huawei Canada, Toronto, ON, Canada, as an Intern, where he created in-lab measurement scripts to characterize a prototype 56-Gb/s SerDes integrated chip. In 2019, he was transferred into the Ph.D. program with the University of Toronto. He also received experience in 7-nm FinFET layout. He is currently conducting research in the area of timing recovery for discrete multitone applications.

MIAD LAGHAEI (Student Member, IEEE) received the B.Sc. degree in electrical engineering from the Sharif University of Technology, Tehran, Iran, in 2018. He is currently pursuing the Ph.D. degree with Huawei Ottawa Research and Development Center, Ottawa, ON, Canada. In the fall of 2018, he was accepted at the M.A.Sc. program with the University of Toronto, Toronto, ON, Canada. In the Fall of 2019, he started his internship in Huawei Ottawa Research and Development Center, to evaluate architecture and design for above 100-Gb/s applications. At the same time, he was also directly transferred to a Ph.D. program. He is currently conducting research in the area of discrete multitone modulation for high-speed wireline applications under the supervision of Prof. A. Sheikholeslami.

HOSSEIN SHAKIBA (Senior Member, IEEE) received the B.Sc. and M.Sc. degrees in electrical engineering from the Department of Electrical and Computer Engineering, Isfahan University of Technology, Iran, in 1985 and 1989, respectively, and the Ph.D. degree in electrical engineering from the Department of Electrical and Computer Engineering, University of Toronto, Toronto, ON, Canada, in 1997. He has over 30 years of teaching, research, design, and management experience in the area of analog circuit and system design for various applications with a focus on wireline communication in the industry and academia. He is currently working on system and circuit design and development for next generation high-performance and high-efficiency serial links with Huawei Canada.

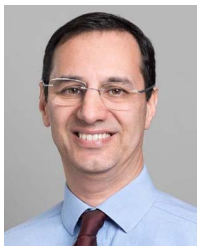

ALI SHEIKHOLESLAMI (Senior Member, IEEE) received the B.Sc. degree from Shiraz University, Iran, in 1990, and the M.A.Sc. and Ph.D. degrees in electrical engineering from the University of Toronto, ON, Canada, in 1994 and 1999, respectively.

In 1999, he joined the Department of Electrical and Computer Engineering, University of Toronto, where he is currently a Professor. He was on Research Sabbatical with Fujitsu Labs from 2005 to 2006, and with Analog Devices, Toronto, from 2012 to 2013. He has coauthored over 70 journal and conference papers, ten patents, and a graduate-level textbook entitled *Understanding Jitter and Phase Noise*. His research interests are in analog and digital integrated circuits, high-speed signaling, and CMOS annealing.

Dr. Sheikholeslami received numerous teaching awards, including the 2005–2006 Early Career Teaching Award and the 2010 Faculty Teaching Award, both from the Faculty of Applied Science and Engineering from the University of Toronto. He served on the Memory Subcommittee of the ISSCC from 2001 to 2004, on the Technology Directions Subcommittee of the ISSCC from 2002 to 2005, and on the Wireline Subcommittee of the ISSCC from 2007 to 2013. He currently serves as the Education Chair for ISSCC and the Vice President, Education, for SSCS, overseeing the SSCS Distinguished Lecturer Program, Webinars, Circuit Contests, and other educational activities. He is an Associate Editor for the *Solid-State Circuits Magazine*, in which he has a regular column entitled *Circuit Intuitions*. He was an Associate Editor for the IEEE TRANSACTIONS ON CIRCUITS AND SYSTEMS—I: REGULAR PAPERS from 2010 to 2012, and the Program Chair for the 2004 IEEE ISMVL. He is a registered Professional Engineer in Ontario, Canada.